Keywords
Hybrid Classification, Nighttime Light, Random Forest, SCATSAT-1, Urban Mapping.

Authors
Binay Kumar Singh[1*], Department of Computer Science, Vivekananda Global University, Jaipur and Department of Remote Sensing & Geoinformatics, Birla Institute of Technology, India.
E-mail: binaykrsingh@bitmesra.ac.in
Orcid Id: 0009-0005-9474-6261

Surendra Yadav[2], Department of Computer Science, Vivekananda Global University, Jaipur, India.
E-mail: surendra.yadav@vgu.ac.in
Orcid Id: 0000-0002-6519-4788

Madan Mohan Agarwal[3], Department of Computer Science, Birla Institute of Technology, India.
E-mail: mmagarwal@bitmesra.ac.in
Orcid Id: 0000-0003-4275-7485

Received:09-06-2026
Revised:15-07-2026
Accepted:23-07-2026
Doi:10.1922/ejprd.v34i5s.1681

An Integrated SCATSAT-1 and VIIRS Nighttime Light approach for Urban Mapping in Arid Zone

Abstract
The atmospheric dust, extreme climate, and cloudy weather conditions during the monsoon season are the major challenges that are facing the urban monitoring in arid and semi-arid regions such as Rajasthan, where optical remote sensing data is often hard to obtain. In view of these limitations, this study suggests a hybrid approach to regional urban mapping in Rajasthan, India, using scatterometer data from the SCATSAT-1 satellite and VIIRS data (NTL). Areas of built-up and non-built up status were obtained using Ku-band backscatter data (σ0) with a spatial resolution of approximately 2 km. A Random Forest (RF) classifier was trained with well distributed data samples from the whole of Rajasthan collected in the month of May 2017. The classification results of SCATSAT-1 radar data were fused with NTL Radiance thresholding to overcome the inherent ambiguity in radar data between rough dry soil and urban structures. The study illustrates how SCATSAT-1 data when combined with NTL data offers a fast and weather-independent solution for a large-scale urban monitoring and sprawl assessment in arid regions.

INTRODUCTION

The Indian Space Research Organisation (ISRO) has developed a scatterometer satellite, named SCATSAT-1, launched in 2016, is a significant improvement in Earth observation by microwave remote sensing in land and vegetation studies. It is a Ku-band (~13.5 GHz) data product that has considerably better spatial resolution (~2 km) than previous scatterometers. Its main advantage is that it can get observations in all weather conditions, regardless of whether the weather is cloudy or bright, since microwave isn't affected by the atmosphere. This allows monitoring of land surfaces consistently day-night, overcoming typical limitations of optical satellite systems.

The main purpose of SCATSAT-1 is to produce backscatter (σ°) measurements, affected by surface roughness, soil moisture and vegetation properties (Duan et al., 2026). This leads to varying responses for various land cover classes (e.g. forests, agricultural fields, barren land, urban areas). The fact that this variability exists is the reason why it is used in land cover classification. The spatial resolution is moderate, but the high temporal frequency enables good temporal monitoring and tracking of seasonal and short term variations, mainly in agriculture areas where surface changes are rapid.

It has been extensively applied to study growth cycles of crops, drought condition analysis and yield prediction (Tripathy & Bhattacharya, 2021; Kaur et al., 2023; Ujjwal Singh et al., 2019). Microwave signals can penetrate dense vegetation and cloudy conditions to provide information, which optical sensors may be unable to provide.

Its features make it ideal for large-scale environmental monitoring and resource management applications, particularly in regions where data is sparse such as India.

From a vegetation monitoring perspective, SCATSAT-1 will be useful for studying sparse and seasonal vegetation in arid regions like the state of Rajasthan. Due to the sensitivity of microwave backscatter to vegetation water content, it can be used to determine crop development, vegetation health and drought stress (Vreugdenhil et al., 2022). The information is particularly useful for those major crops such as bajra (pearl millet), wheat and mustard that are widely grown in the region. Further, it can also be used for the monitoring of rangelands and grazing areas, which is essential for the livestock-dependent communities (Singh et al., 2019; Tripathy & Bhattacharya, 2021; Kaur et al., 2023).

2. Study Area

For the present study, the state of Rajasthan was chosen for the analysis of the Urban sprawls using SCATSAT-1 data and VIIRS Nighttime Light (NTL). Rajasthan is located in the north west of India and is the largest state in the country with an area of approximately 342239 Sq. km (as per Rajasthan government website). It is very heterogenous with extreme environmental conditions and the dry and semidry regions of Thar desert are predominant in the western and north western parts of the region which gradually reduces to eastern parts of the region where seasonal vegetation is sparse.

In 2017 (October to May), several spaceborne data were fused in order to create a complete hybrid land classification system (Fabris et al., 2022). Combination and extraction of various spaceborne datasets from October 2017 to May 2017 yielded a strong hybrid land classification system. The characteristics of the primary and auxiliary layers of data utilized are described below:

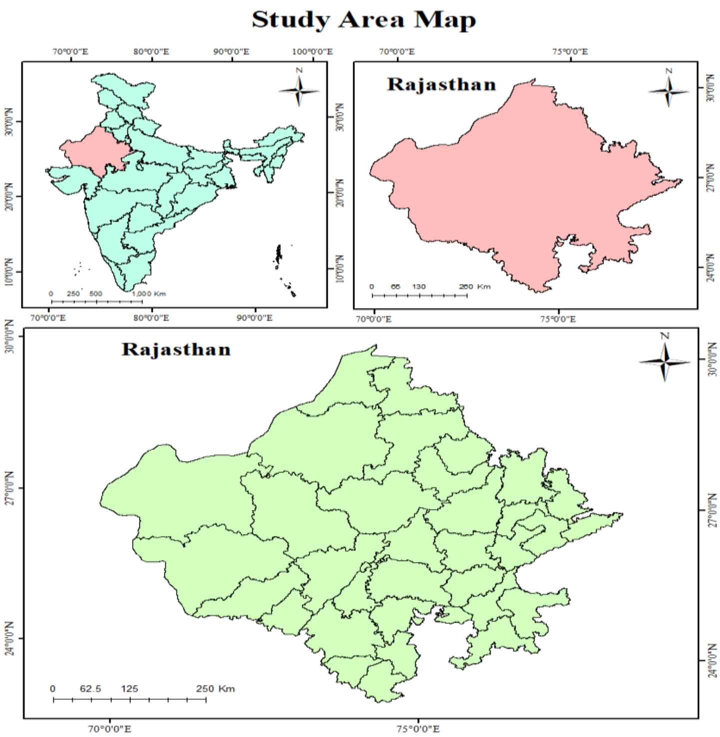

Figure 1: Study Area Map

Table. 1 Data and their Product used

Data / Sensor	Product	Spatial Resolution	Role in Study	Processing Applied
SCATSAT-1	Level-2 Backscatter	~2 km	Primary classification feature for RF model	Read via rasterio · nodata masked to NaN · SCAT_SCALE computed
Suomi-NPP VIIRS	VCMSLCFG Monthly v1	~500 m	NTL ≥ 3.0 DN confirms Buildup class	Mean monthly composite · bilinear reproject to SCATSAT grid
GEE Training Points	Visual interpretation samples	Point locations	80% train / 20% test for RF ·	Stratified split · merged on pt_id with raster values

3. Materials and Methods

i) SCATSAT-1 Backscatter

The Indian Space Research Organisation (ISRO) built and operated a scatterometer, SCATSAT-1, that operates at the Ku-band (~13.515 GHz) and measures the normalized radar backscatter (sigma-naught, in decibels) of the Earth's surface. The surface roughness and soil moisture conditions and vegetation density affect this backscatter signal. The user has directly provided a pre-processed GeoTIFF file of the composite image of the SCATSAT-1 over Rajasthan from October 2017 as the main data set for the present study.

Once the dataset was loaded, the raster array was converted to float32 to allow for proper analysis of the data (Ribeiro, 2025), and it was ensured that all pixels that were determined to be NoData were replaced with NaN to ensure proper handling during the analyses.

ii) VIIRS Nighttime Light (VCMSLCFG)

The VIIRS Day/Night Band (DNB) composites (NOAA/VIIRS/DNB/MONTHLY_V1/VCMSLCFG) were used to download monthly nighttime light radiance data from Google Earth Engine (GEE) (Iyoob et al., 2026). For October 2017, the average radiance over the band (also known as the average rad band or "avg_rad" in the code) was extracted, which is commonly referred to as "avg_rad" or "DN values" in existing literature. The image produced was exported and reprojected like the NDVI data, to conform to the grid of SCATSAT-1. The threshold value was determined as NTL_THRESH = 3.0 DN as this is considered as a typical threshold value for built-up areas.

Training Sample Points

Training samples were created using visual interpretation and added as a FeatureCollection. The attribute Class was used for each sample point with values assigned as 0: built-up areas, 1: vegetation, and 2: barren land.

A random identifier (pt_id) has been added to each feature to ensure the reproducibility. FeatureCollection.The seed number of 42 is used for randomColumn(). At each location, spectral variables (NDVI, NTL, etc.) were sampled as well as environmental variables.Image.sampleRegions() at the scale of SCATSAT. Using rasterio.transform.rowcol(), geographic coordinates were transformed into raster indices (row and column) in order to extract the corresponding backscatter values (in dB) in the SCATSAT-1 image.

Spatial restriction of the dataset was done using the filter Bounds function with the study area shapefile (AOI). Temporal filtering was then used to select imagery for three representative months (January, May and October 2017). The images selected were loaded from the Image Collection, then a series of pre-processing operations such as mask quality and radiometric scaling were performed (Jia et al., 2024).

Training samples were created as Feature Collections in Google Earth Engine (GEE) for each month. A built-up/non-built up binary classification (Li et al., 2025) was created for each sample point with 0 indicating built-up areas and 1 indicating non-built up regions. These labels were created by extracting optical imagery and NTL patterns and visually interpreting them. The Feature Collections were then combined and exported to GEE assets each month. Further, the NTL layers and the barren land extracted datasets were saved as separate files to Google Drive for each of the three months.

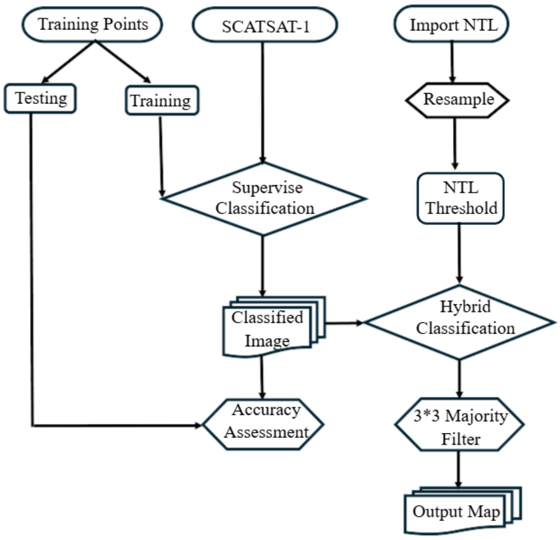

Figure 2: Workflow implementation

Training samples

The training sample points were obtained from the GEE assets and the SCATSAT-1 data were downloaded from the local storage along with the NTL datasets. The important information from the compiled data was then split into training (80%) and test (20%) data sets with stratified random sampling (Sadaiyandi et al., 2023). This will result in class proportions being equal in both sub-sets, which will reduce class imbalance problems when the models are evaluated. The test subset was kept for the evaluation and the training subset was kept for the model fitting.

The NTL raster was resampled to the resolution of the SCATSAT-1 (~2 km resolution) grid for spatial compatibility. To compare the datasets at the pixel scale, they need to have the same spatial resolution and alignment (Wang et al., 2021). For continuous NTL values bilinear interpolation was performed, balancing smoothness and efficiency via averaging neighbouring pixel values.

Feature Scaling

Although Random Forest algorithms are generally insensitive to feature scaling, a Standard Scaler was applied to maintain methodological consistency (Herrera et al., 2025). This transformation standardizes the SCATSAT backscatter values by centering them around zero and scaling them to unit variance. Importantly, the scaler was fitted only on the training dataset and subsequently applied to the test dataset. This practice prevents data leakage and ensures that model evaluation remains unbiased.

Random Forest Classification

Ensemble learning method Random Forest (RF) algorithm was used for classification (Aziz et al., 2024). Builds several decision trees, each using threshold-based rules from the input feature for prediction. For this scenario, a single continuous variable, namely backscatter values in dB from SCATSAT-1 was used for training the model.

NTL values were derived at training sites, but were deliberately separated from input to the RF model and added to the final hybrid classification and validation steps. In this design, classification is based on microwave backscatter alone, and is independent of auxiliary datasets, and not circular.

The model was built with 300 trees and the dataset split into 20% stratified test dataset and 80% training dataset. The classified image contains only three classes: 0 (Built-up), 1 (Vegetation), and 2 (Barren) for valid pixels with NoData (-1) for invalid pixels. This produces an RF classification map which can be used as input to the hybrid classification stage and as accuracy assessment for the classification independently.

To increase the interpretability, the decision boundaries were determined by analyzing a large number of values of the backscatter and by observing the change between the classes predicted by them (Zargari et al., 2023). This helps to understand the relationship between the different ranges of backscatter and the different types of land cover. For the evaluation of the model performance, several parameters of the confusion matrix were used, such as the Overall Accuracy (OA), Cohen’s Kappa coefficient, Producer's Accuracy (PA), User's Accuracy (UA), and omission and commission errors.

Nighttime Light Thresholding

A fixed threshold value of NTL_THRESH = 3.0 DN (nW/cm²/sr) was adopted to identify built-up areas. This threshold is consistent with established practices in urban mapping studies using VIIRS data, where radiance values above approximately 2–5 nW/cm²/sr are typically associated with urban or developed regions.

In the context of Rajasthan, which is largely rural and arid, this threshold effectively isolates urban areas, industrial zones, and densely populated settlements (Joshi and Gupta, 2022). Pixels with radiance values equal to or exceeding this threshold were classified as built-up for confirmation purposes.

Full-Image Prediction

After the model training, the RF model was applied to the whole SCATSAT-1 dataset (Singh et al., 2020). The backscatter raster was first converted to a one-dimensional array and then had valid (non-NaN) pixels selected. These values were scaled with the fitted scaler,

and then fed into the RF model one batch at a time. The class labels predicted were then reconverted to the original two dimensional raster format.
The resulting classification map contains class labels for valid pixels and NoData values are retained. This RF output was used for subsequent classification in hybrid format as well as independent validation to ensure no bias was added through the use of NTL data in later stages.

Hybrid Classification
The hybrid classification approach addresses the inherent ambiguity of radar-based classification, where backscatter signals are influenced by multiple surface properties simultaneously (Meng et al., 2024). To reduce misclassification, RF predictions were validated using independent spectral information from NTL data.
A pixel was classified as built-up only if it satisfied two conditions: it was predicted as built-up by the RF model, and its corresponding NTL value exceeded the defined threshold (≥ 3.0 DN). This dual-conditioning approach ensures that only pixels with strong and consistent urban signatures are classified as built-up. The use of NTL as a confirmation layer is particularly effective, as human settlements exhibit distinct and spatially coherent nighttime radiance patterns rarely observed in non-urban areas.

Spatial Post-Processing: 3×3 Majority Filter
Moderate-resolution radar classification data can sometimes result in “salt-and-pepper” noise, where individual pixels are classified into different classes from the surrounding area (Merchant, 2025). In order to reduce this effect, a 3×3 majority filter was used, which replaces each pixel's class label with the most common class label in the neighborhood of a pixel. This filters out the random noise, but does not alter the meaningful spatial patterns.
The filter was applied via a python function scipy.ndimage.generic_filter() in the custom mode. NoData pixels were replaced with NaN(Not a number) prior to filtering to not be included in neighborhood calculation. Following the filter process, the filtered values were converted to integer again and the original NoData mask restored. The percentage change of pixels after filtering was also computed as an indicator of classification noise, typical range being 0.5-3%.

Accuracy Assessment
Stratified 5-fold cross-validation was applied to the binary training dataset consisting of 200 samples (100 Built-up and 100 Non-built-up) for each seasonal subset. This approach provides a more reliable estimate of model performance by evaluating the classifier across five independent train–test partitions and averaging the results, thereby reducing dependence on any single data split. Table 2 presents the Overall Accuracy (OA) and Cohen’s Kappa (κ) values obtained for each fold across all seasons, along with their corresponding mean and standard deviation.

Table 2. RF 5-fold cross-validation: Overall Accuracy (OA%) and Cohen's Kappa (κ) per fold.

Fold	May OA%	May κ
1	95.00%	0.9000
2	82.50%	0.6500
3	82.50%	0.6500
4	85.00%	0.7000
5	75.00%	0.5000
Mean	84.00%	0.6800
Std	±6.44%	—

For the May dataset, the mean cross-validation accuracy reached 84.00% (±6.44%), with a Kappa coefficient of 0.6800, indicating a substantial level of agreement. However, the relatively high standard deviation (±6.44%) suggests noticeable variability between folds. This variation is likely attributable to the limited number of built-up training samples and the spectral similarity between built-up surfaces and dry agricultural land during the summer period.

Table 3. Per-class Producer's Accuracy (PA%) and User's Accuracy (UA%) from RF 5-fold

Class	May PA%	May UA%
Non-built-up	84.00%	84.00%
Built-up	84.00%	84.00%

The classification performance for both classes was balanced as they had the same Producer's Accuracy (PA) of 84.00% in this season.The classification performance of the two classes was same, both having Producer's Accuracy (PA) of 84.00% in this season. In parallel, this symmetry highlights the natural confusions between dry soil surfaces and built-up surfaces in dry environments, where their spectral signatures are not easily distinguishable.

The last classification shows that only a small number of pixels (528 pixels or 0.68% of the study area) are in built-up areas. This small spatial scale is well explained by the geographical nature of Rajasthan as the largest state in India, but has rather low population density. The Thar Desert, semi-arid lands and dryland agriculture dominate much of the region. Only a small percentage of the state's land area (342,239 km²) is covered by urban areas like Jaipur, Jodhpur, Kota, Ajmer and Bikaner. Also, the moderate spatial resolution of SCATSAT-1 (~2 km) limits the identification of urban built-up areas mostly to high-density urban cores where individual pixels are sufficiently dominated by urban built-up area.

4. Results and Discussion

The principle behind microwave mapping of urban regions is that there are more corner reflector effects in densely built-up regions, which are caused by the interaction of vertical structures (walls, etc.) and horizontal surfaces (roads, etc.). Therefore, these areas have higher sigma-naught (σ°) values than the other land cover types in the area, such as those in rural, agricultural and desert areas. The Ku-band (~13.515 GHz) backscatter data from the SCATSAT-1 mission over the area of Rajasthan for May 2017 clearly exhibit this theoretical expectation, with a good demarcation between urban and non-urban areas.

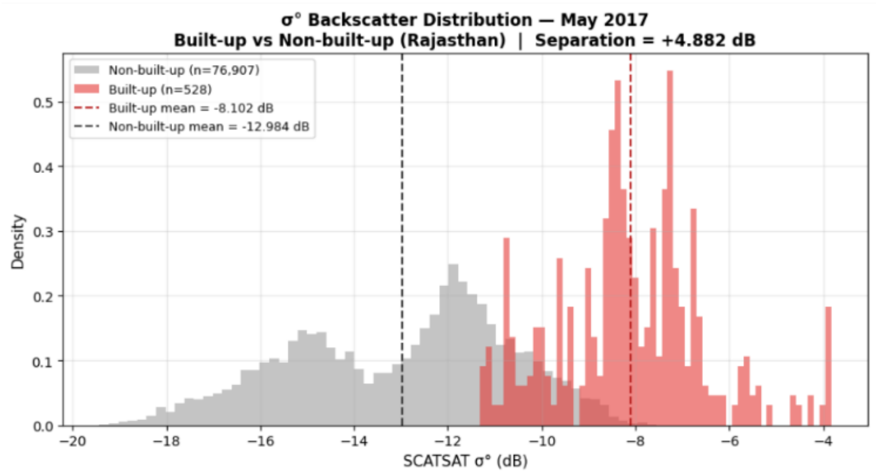

Figure 3: σ° (Backscatter Distribution Histogram — May 2017

The built-up class has a mean value of −8.102 dB as displayed in the distribution histogram of the σ° backscatter shown in Figure 3 (n = 528 pixels). However, the non-built-up areas, which are mainly comprised of smooth desert sand, exposed alluvial plains and post-harvest agricultural fields have a much lower mean value of −12.984 dB. The resulting separation was around +4.882 dB (Cohen's d = +2.457) which is statistically significant and physically meaningful. This difference is due to the fact that the scattering in the desert is mostly specular and the scattering in urban areas is mostly double bounce scattering, which is more common in bigger cities like Kota, Ajmer, Jodhpur and Jaipur.

The nature of these observations in May are double edged (Collins et al., 2020). On the other hand, during this time period the difference in the respective σ° values for built-up and non-built-up classes is the highest, enabling urban areas to be easily identifiable in the low-backscatter background of the Thar desert. However, there is some ambiguity during the dry season. The backscatters from harvested agricultural fields in some eastern parts of the Indian state of Rajasthan are relatively high because of increased surface roughness. This leads to a certain overlap of built-up backscatter values to the lower end of the range. The model performance for the Random Forest model is also ambiguous with the 5-fold cross validation showing the lowest performance for the season (OA = 84.00%, κ = 0.68) despite the strong physical separation that was observed in the data.

This is further confirmed by the decision boundary obtained from the Random Forest classifier (Wang et al., 2021b). The distribution of pixels with σ° values that are significantly lower than −10 dB was consistent with being classed as built up, and is in agreement with previous results in Ku-band urban backscatter studies. The integration of this threshold with VIIRS nighttime light (NTL) confirmation proved effective in reducing misclassification. In particular, surfaces with high backscatters but lacking significant nighttime radiance—such as rocky terrain or recently irrigated fields—were successfully excluded from the built-up class.

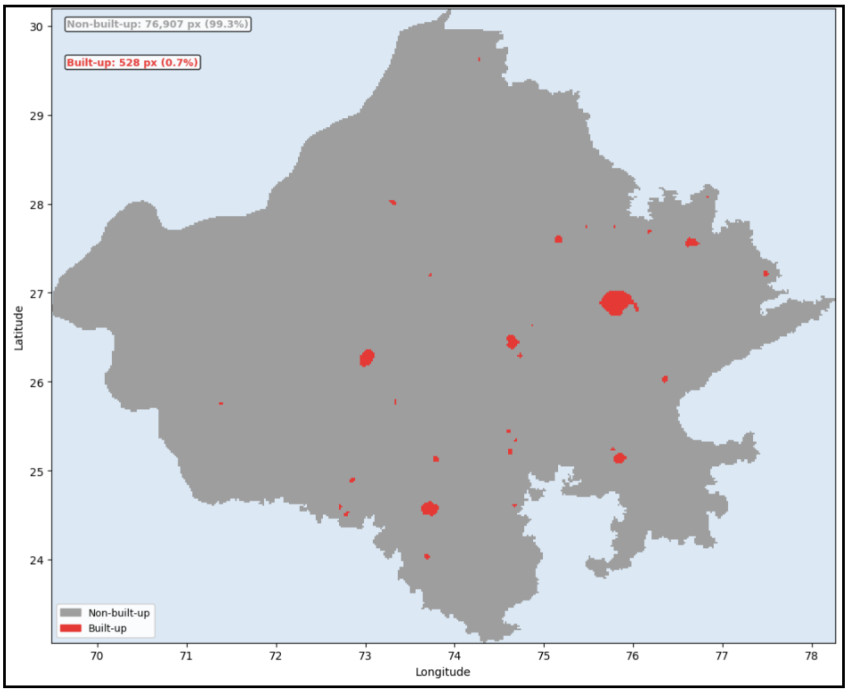

Figure 4: Built-up Map of Rajasthan (May 17)

Spatial Distribution of Classified Built-up Areas

In May 2017 a total of 528 pixels were classified as built-up which is about 0.68% of the valid study area in the state of Rajasthan. The percent of this proportion seems low, but it is in line with the spatial and demographical characteristics of the region. Rajasthan is the largest state in India (~342,239 km²) which has low population density, where majority of the area is characterized by desert landscapes, semi-arid vegetation, and dryland agriculture. This means that there are only limited areas of urban settlements.

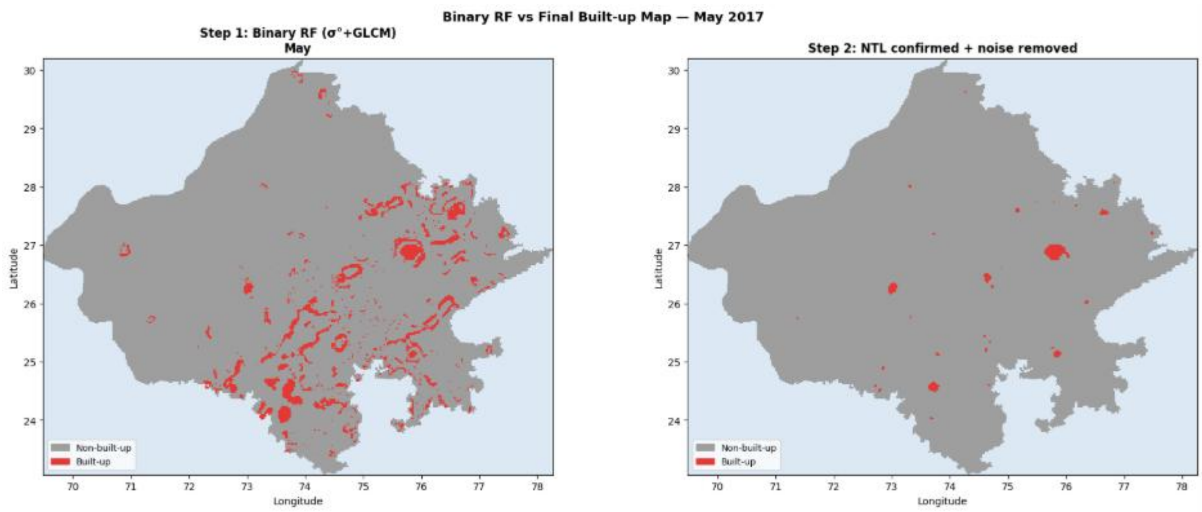

Figure 5: Binary RF vs. Final Built-up Map — May 2017

The spatial distribution (Figure 4: final built-up map; Figure 5: binary RF vs. NTL-confirmed classification) shows some interesting patterns. The most prominent and continuous urban population is located near latitude 26.9 N and longitude 75.8 E, which is essentially the location of the state capital and biggest cities of Jaipur. The areas are clearly visible on the Random Forest model and also on the NTL based confirmation and the radiance values are well above the defined threshold.

Further clusters are seen around Jodhpur, Kota, Ajmer and Bikaner. Although the spatial resolution in urban areas is relatively coarse (around 2 km), the urban areas are well captured showing the potential of SCATSAT-1 to capture major and secondary towns/cities on regional scale.

The relatively built-up areas, which are mainly in the western and northwestern parts and are mainly in the Thar Desert in the districts of Jaisalmer and Barmer, are mostly lacking in built-up pixels. This is in line with the actual ground situation, with the smooth desert surfaces giving very low backscatter levels making them distinguishable from urban signatures.

The initial Random Forest results (left panel in Figure 3) and the final NTL validated map (right panel in Figure 3) show both that there is an improvement in classification quality. The first RF classification reveals isolated high backscatter areas in SE Rajasthan, possibly related to rough ground and cropland, particularly in the agricultural areas. The NTL confirmation stage filters out these false positives and leaves only those pixels with high backscatter and a large radiances measured during the night—properties typical of built-up areas.
The 3×3 majority filter was then applied to further refine the image, enhancing the spatial coherence of urban areas and minimizing salt-and-pepper noise.The 3×3 majority filter was then applied to further refine the image, making the urban areas more spatially coherent and reducing the salt-and-pepper noise in the image. Classification noise (changing classification of pixels) varied between about 0.5% and 3% for this step, which is considered to be of moderate size for microwave data at this spatial resolution.

Comparison with JRC Global Human Settlement Layer (GHS-BUILT-S)
The built-up map derived from SCATSAT-1 data has been compared to the built-up map derived from JRC Global Human Settlement Layer Built-up Surface dataset (GHS-BUILT-S, 10 m resolution, P2023A epoch 2020; collection JRC/GHSL/P2023A/GHS_BUILT_S_10m) to evaluate the spatial reliability of the classification beyond the point-based accuracy metrics. It is one of the most robust urban extent product made available for the global extent so far that is provided by using multi-temporal Sentinel-1 and Sentinel-2 observations alongside machine learning techniques.

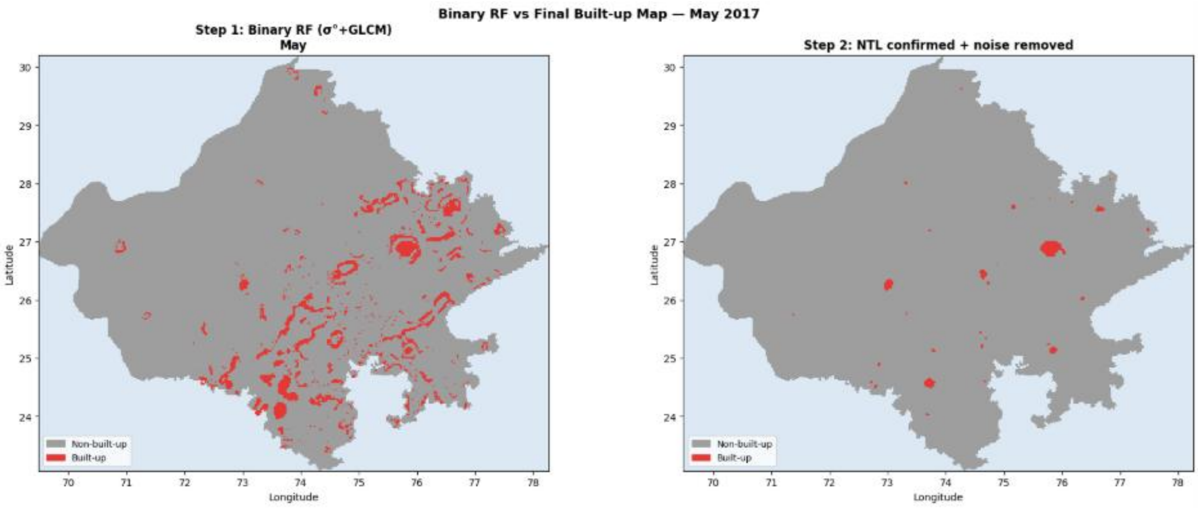

Figure 6: Classified Built-up vs. Built-up Product (GHS-BUILT-S) — RAJASTHAN

The inset panels presented in Figure 6 illustrate a direct spatial comparison between SCATSAT-1-derived built-up pixels (displayed in red/dark red as "Built-up masked") and the GHS-BUILT-S dataset (shown in orange). Several key patterns can be observed from this overlay.

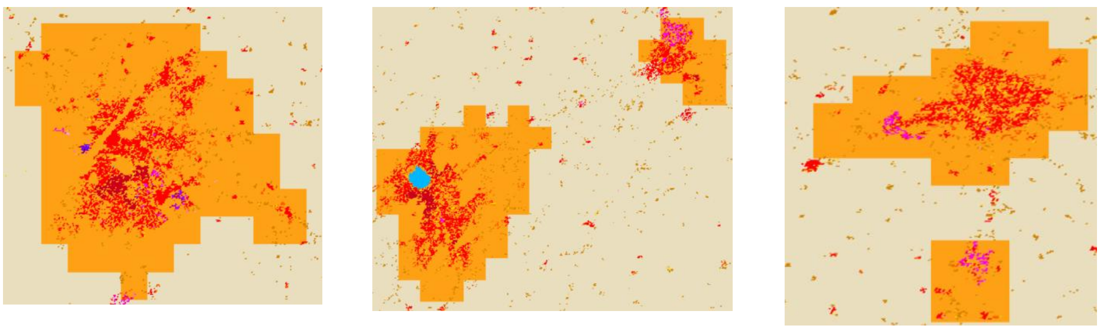

ejprd.org - Published by Riset Publishing Services LLC

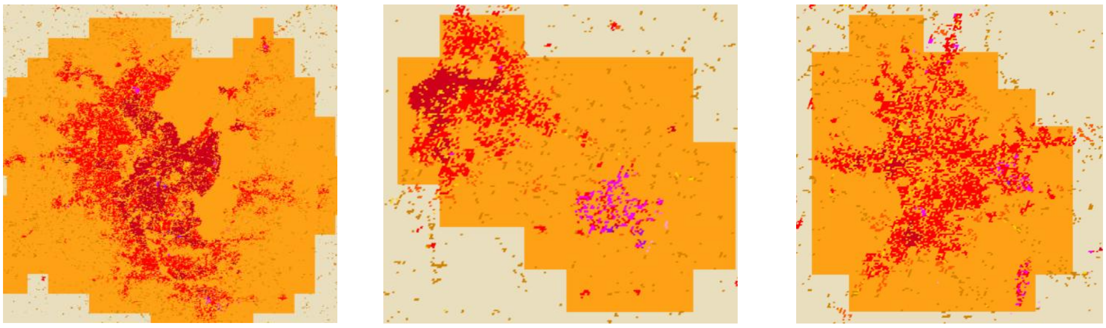

Figure 7: Regional Urban Core Validation Panels Against GHS-BUILT-S Reference Product

It is an important agreement because of the high spatial resolution disparities of the two data sets. GHS-BUILT-S has a fine resolution of 10 m, which is able to capture individual buildings and detailed urban structures, while SCATSAT-1 has a resolution of around 2 km and is able to detect aggregated radar responses over large areas. Yet, the coherence of the spatial patterns indicates that the backscatter microwave signature may be sufficiently different from urban to the rural areas to be recognizable even at coarse spatial resolution.

Table 4. Comparative summary: SCATSAT-1 hybrid classification vs. JRC GHS-BUILT-S product

Metric	SCATSAT-1 Hybrid Classification	GHS-BUILT-S (Reference)
Native Resolution	~2 km	10 m
Data Type	Ku-band SAR backscatter + VIIRS NTL	Sentinel-1 SAR + Sentinel-2 optical
Built-up pixels (Rajasthan)	528 px (0.68%)	Higher areal coverage (finer resolution)
Major cities detected	Jaipur, Jodhpur, Kota, Ajmer, Bikaner	All cities + suburbs + villages
Weather independence	Full (microwave, day/night)	Partial (optical component cloud-sensitive)
Temporal frequency	Daily revisit	Monthly composites
Spatial commission errors	Very low (NTL-gated)	Very low (multi-source)
Spatial omission at periphery	Moderate–High (resolution limit)	Low (fine resolution)

5. Conclusions

This study demonstrates the potential use of SCATSAT-1 Ku-band scatterometer data in conjunction with VIIRS Nighttime Light (NTL) data in a hybrid Random Forest framework, for mapping built-up areas for the sake of arid and semi-arid Rajasthan. The Random Forest model is used to detect potential built-up areas based on their scattering properties and the NTL layer is used as an independent validation to ensure that there is human activity detected by the nighttime illumination.

The joint analysis produced an Overall Accuracy of 92.00% and a Kappa value of 0.84, which is definitely better than the Random Forest model alone (84.00%). This is a nice improvement that shows how important the integration of several data sources is when dealing with moderate-resolution data.

A simple 3×3 majority filter was applied for further improvement of the final output that minimized isolated misclassified pixels and resulted in more continuous urban patches.

To conclude, it can be concluded that SCATSAT-1 can be used effectively to map built-up areas in combination with proper classification techniques using other supporting datasets. The hybrid method had the highest accuracy and it generated results that were very similar to the known pattern in urban areas throughout Rajasthan.

The results indicate that coarse scale microwave data should not be ignored for urban studies. When applied judiciously, and in conjunction with other sources of data, it can be a source of reliable and useful information for large-scale mapping. This is also a valuable basis for further research and for the creation of better remote sensing techniques for urban monitoring and environmental management.

References

1. Duan, P., Zhao, T., Lü, H., Lang, S., Zheng, J., Bai, Y., Peng, Z., Wagner, W., Guo, P., Shi, H., Sun, C., Jia, L., Zhu, D., Dong, X., & Shi, J. (2026). A new addition to global soil moisture mapping: CFOSAT scatterometer algorithm development and validation. IEEE Journal of Selected Topics in Applied Earth Observations and Remote Sensing, 19, 2439–2460.

https://doi.org/10.1109/JSTARS.2025.3645399

2. Iyoob, A. L., Zahir, I. L. M., Suthakaran, S., & Fowzul Ameer, M. L. (2026). Machine learning-based urban nighttime light intensity analysis in Sri Lanka using VIIRS images. Lecture Notes in Networks and Systems, 51–67. https://doi.org/10.1007/978-3-032-09825-2_5
3. Singh B K, Yadav S & Agarwal M M; (2026). Integration of SCATSAT Data and Unsupervised Learning for Accurate Land Use/Land Cover Characterization in Rajasthan; International Journal of Computer Information Systems and Industrial Management Applications; ISSN 2150-7988 Volume 18(9s) pp. 1145-1157.
4. https://doi.org/10.70917/ijcisim-2026-3543
5. Rinaldi, V., & Ghandehari, M. (2026). Characterizing urban form archetypes through landscape and morphology parameterization and dimensionality reduction. International Journal of Digital Earth, 19(1). https://doi.org/10.1080/17538947.2026.2616955
6. Singh B K, Yadav S & Agarwal M M; (2026). Geoai-driven land use/land cover characterization of Rajasthan using scatsat data; International Journal of Computer Information Systems and Industrial Management Applications; ISSN 2150-7988 Volume 18(10s) pp. 450-466.
7. https://doi.org/10.70917/ijcisim-2026-3628
8. Herrera, M., Vilas, S., Silva, A. P., Ferreira, E., Godoy, R. V., Ambrosio, L. A., & Becker, M. (2025). The impact of feature scaling in machine learning: Effects on regression and classification tasks. IEEE Access, 1–1. https://doi.org/10.1109/ACCESS.2025.3635541
9. Li, Y., Zhong, X., Liu, H., Liao, M., Lu, Y., & Liu, B. (2025). Urban built-up area extraction using triangle threshold algorithm and naive Bayes classification model with multidata fusion. Scientific Reports, 15(1). https://doi.org/10.1038/s41598-025-23986-w
10. Merchant, M. (2025). Enhanced characterization of wet Arctic ecosystems using Earth observation satellite data and machine learning [Master's thesis, University of Guelph]. https://atrium.lib.uoguelph.ca/items/c04bd656-7781-4222-b383-3c78dadd8ce2
11. Nathawat, R., Singh, S. K., Sajan, B., Pareek, M., Kanga, S., Đurin, B., Kantamaneni, K., & Rathnayake, U. (2025). Integrating cloud-based geospatial analysis for understanding spatio-temporal drought dynamics and microclimate variability in Rajasthan: Implications for urban development planning. Journal of the Indian Society of Remote Sensing. https://doi.org/10.1007/s12524-025-02139-6
12. Nekruz Gulahmadov, & Parvizi Hotam. (2025). Assessing the impact of urbanization on air pollution and land surface temperature using remote sensing data in Google Earth Engine: A case study of Tehran Province (2018–2022). Ecological Questions, 36(4), 1–21. https://doi.org/10.12775/eq.2025.038
13. Aziz, G., Minallah, N., Saeed, A., Frnda, J., & Khan, W. (2024). Remote sensing based forest cover classification using machine learning. Scientific Reports, 14(1), 69. https://doi.org/10.1038/s41598-023-50863-1
14. Farhad Samadzadegan, Toosi, A., & Javan, F. D. (2024). A critical review on multi-sensor and multi-platform remote sensing data fusion approaches: Current status and prospects. International Journal of Remote Sensing, 1–76. https://doi.org/10.1080/01431161.2024.2429784
15. Guan, S., Liu, B., Chen, S., Wu, Y., Wang,F., Liu, X., & Wei, R. (2024). Adaptive median filter salt and pepper noise suppression approach for common path coherent dispersion spectrometer. Scientific Reports, 14(1). https://doi.org/10.1038/s41598-024-66649-y
16. Meng, L., Yan, C., Lv, S., Sun, H., Xue, S., Li, Q., Zhou, L., Edwing, D., Edwing, K., Geng, X., Wang, Y., & Yan, X. (2024). Synthetic aperture radar for geosciences. Reviews of Geophysics, 62(3). https://doi.org/10.1029/2023RG000821
17. Xiao, Y., Huang, J., Weng, W., Huang, R., Shao, Q., Zhou, C., & Li, S. (2024). Class imbalance: A crucial factor affecting the performance of tea plantations mapping by machine learning. International Journal of Applied Earth Observation and Geoinformation, 129, 103849. https://doi.org/10.1016/j.jag.2024.103849
18. Sadaiyandi, J., Arumugam, P., Sangaiah, A. K., & Zhang, C. (2023). Stratified sampling-based deep learning approach to increase prediction accuracy of unbalanced dataset. Electronics, 12(21), 4423. https://doi.org/10.3390/electronics12214423
19. Sengani, D., Ramoelo, A., & Archer, E. (2023). A review of fusion framework using optical sensors and synthetic aperture radar imagery to detect and map land degradation and sustainable land management in the semi-arid regions. Geocarto International, 38(1). https://doi.org/10.1080/10106049.2023.2278325
20. Zargari, S., Hakimi, A., Rezaei, F., Tellambura, C., & Maaref, A. (2023). Signal detection in ambient backscatter systems: Fundamentals, methods, and trends. IEEE Access, 11, 140287–140324. https://doi.org/10.1109/ACCESS.2023.3341416
21. Fabris, M., Battaglia, M., Chen, X., Menin, A., Monego, M., & Floris, M. (2022). An integrated InSAR and GNSS approach to

monitor land subsidence in the Po River Delta (Italy). Remote Sensing, 14(21), 5578. https://doi.org/10.3390/rs14215578
22. Joshi, A. K., & Gupta, N. (2022). Urbanisation and its impact on environment: A case study of central region of Rajasthan. Central Asian Journal of Theoretical and Applied Science, 3(10), 66–73.
23. https://cajotas.casjournal.org/index.php/CAJOTAS/article/view/940
24. Vreugdenhil, M., Greimeister-Pfeil, I., Preimesberger, W., Camici, S., Dorigo, W., Enenkel, M., van der Schalie, R., Steele-Dunne, S., & Wagner, W. (2022). Microwave remote sensing for agricultural drought monitoring: Recent developments and challenges. Frontiers in Water, 4. https://doi.org/10.3389/frwa.2022.1045451
25. Wang, W., Zhou, T., Yu, F., Dai, J., Konukoglu, E., & Van Gool, L. (2021a). Exploring cross-image pixel contrast for semantic segmentation. In Proceedings of the IEEE/CVF International Conference on Computer Vision (pp. 7303–7313). http://openaccess.thecvf.com/content/ICCV2021/html/Wang_Exploring_Cross_Image_Pixel_Contrast_for_Semantic_Segmentation_ICCV_2021_paper.html
26. Wang, X., Zhai, M., Ren, Z., Ren, H., Li, M., Quan, D., Chen, L., & Qiu, L. (2021b).
27. Singh, S., Tiwari, R. K., Sood, V., & Gusain, H. S. (2020). Detection and validation of spatiotemporal snow cover variability in the Himalayas using Ku-band (13.5 GHz) SCATSAT-1 data. International Journal of Remote Sensing, 42(3), 805–815. https://doi.org/10.1080/2150704X.2020.1825866